frontiers | Frontiers in Bioengineering and Biotechnology

TYPE Original Research
PUBLISHED 20 May 2025
DOI 10.3389/fbioe.2025.1608188

OPEN ACCESS

EDITED BY
Mahendran Sekar,
Monash University Malaysia, Malaysia

REVIEWED BY
Spase Stojanov,
Institut Jožef Stefan (IJS), Slovenia
Gaurav Pandey,
Louisiana Tech University, United States

*CORRESPONDENCE
Yu Zhang,
zhangydr@126.com

RECEIVED 08 April 2025
ACCEPTED 08 May 2025
PUBLISHED 20 May 2025

CITATION
Zhang Y, Liu J, Li S, Zhou J, Liu J and Huang Y (2025) pH-triggered CS@ZnO_2 nanocomposites: Self-activated ROS generation for efficient bacterial eradication. *Front. Bioeng. Biotechnol.* 13:1608188. doi: 10.3389/fbioe.2025.1608188

pH-triggered CS@ZnO_2 nanocomposites: Self-activated ROS generation for efficient bacterial eradication

Yu Zhang*, Jun Liu, Sha Li, Jinhua Zhou, Jiushan Liu and Yan Huang

Department of Emergency, The Fourth Hospital of Changsha (Integrated Traditional Chinese and Western Medicine Hospital of Changsha), Changsha, Hunan, China

Functional nanomaterials based on reactive oxygen species (ROS) have attracted considerable attention in the treatment of bacterial infections, owing to their high sterilization efficiency and low tendency to induce drug resistance. Natural polymers, known for their excellent biocompatibility, have been widely used in the development of antibacterial dressings. In this study, chitosan-zinc peroxide composite dressing (CS@ZnO_2) was synthesized using zinc acetate and chitosan as primary raw materials, and comprehensive characterizations were performed. Under the slightly acidic conditions of bacterial infections, CS@ZnO_2 could self-decompose to release H_2O_2 and produce large amount of ROS, which would cause damage to bacteria. The *in vitro* antibacterial properties of CS@ZnO_2 were investigated using *Escherichia coli* (*E. coli*) and *Staphylococcus aureus* (*S. aureus*) as representative pathogens. The results demonstrated that CS@ZnO_2 exhibited potent antibacterial efficacy against both *S. aureus* and *E. coli*. This research provides an important theoretical foundation and technical support for the development of novel antibacterial materials, and has the potential to improve the efficacy of treatments for bacterial infections in the future.

KEYWORDS

chitosan, zinc peroxide, self-supply H_2O_2, reactive oxygen species, antibacterial

1 Introduction

Bacterial infection is a major threat to human health. The discovery and development of antibiotics in the 20th century revolutionized medicine by drastically reducing the fatality rates associated with bacterial infectious diseases (Davies and Davies, 2010; Cook and Wright, 2022). However, the widespread and sometimes inappropriate use of antibiotics has led to an alarming rise in bacterial drug resistance. Bacteria have evolved mechanisms to survive exposure to antibiotics, rendering many traditional treatments less effective or even obsolete (Theuretzbacher et al., 2023). The growing prevalence of resistant strains necessitates the exploration of new antibacterial agents. In response to this challenge, researchers are investigating innovative materials and therapies that can combat bacteria in novel ways. Nanomaterials, including precious metals like silver and gold, non-metallic compounds, and antibacterial hydrogels, have shown remarkable promise due to their unique properties. These materials can disrupt bacterial cell walls, inhibit bacterial growth, and prevent biofilm formation, making them highly effective against both drug-sensitive and resistant strains (Xin et al., 2019; Makabenta et al., 2021; Stojanov et al., 2022; Chen

et al., 2024; Yang et al., 2024). Although nano-antibacterial agents provide new strategies for combating bacterial infections, developing efficient and safe nano-antibacterial agents remains an arduous task.

Among the numerous emerging antibacterial strategies, the controllable generation of reactive oxygen species (ROS) for combating bacteria is attracting increasing attention. One of the key advantages of using ROS-based approaches is that they generally do not induce drug resistance, a significant concern with traditional antibiotics. This is because ROS attack multiple cellular targets simultaneously, making it difficult for bacteria to develop resistance mechanisms (Xie et al., 2020; Bi et al., 2022; Cao et al., 2022; Hwang et al., 2022; Sun et al., 2024). Since bacteria possess an endogenous antioxidant defense system to detoxify abnormal external oxidants (Dong and Wang, 2023). Hence, the prerequisite for ROS to be effective is to ensure that their content exceeds the bacterial tolerance threshold. To achieve the desired antibacterial effect, developing nanomaterials that can generate ROS efficiently is of paramount importance. Nanomaterials offer several advantages in this context. Their high surface area-to-volume ratio allows for enhanced reactivity, enabling more efficient production of ROS. Additionally, nanomaterials can be engineered to respond to specific environmental cues, such as pH changes, thereby providing targeted and controlled release of ROS directly at the site of infection.

Metal peroxides are efficient alternative sources of H_2O_2, and their physicochemical properties are more stable than those of H_2O_2 (Elbahri et al., 2017; Bai et al., 2022; Liu et al., 2022). They are composed of metal ions and peroxide groups and can reversibly release H_2O_2 in an acidic environment (Lin et al., 2019; Zhang et al., 2022). In recent years, nanomaterials have received attention due to their significant effects on antibacterial applications. Nevertheless, these materials still face challenges such as stability, preparation difficulty, and biosafety in practical applications. To solve these problems, this study aimed to synthesize a metal-based nanomaterial and investigate its antibacterial performance. The specific research contents are as follows: A chitosan-zinc peroxide composite dressing (CS@ZnO_2) was prepared using zinc acetate, hydrogen peroxide, sodium hydroxide, and chitosan as raw materials. Through the characterization and analysis of the synthesized CS@ZnO_2, the structural characteristics and performance parameters were elucidated. Then, *in vitro* antibacterial experiments against *E. coli* (*Escherichia coli*) and *Staphylococcus aureus* (*Staphylococcus aureus*) were conducted to validate the antibacterial performance of CS@ZnO_2.

2 Experimental section

2.1 Preparation of ZnO_2

0.5 g of zinc acetate dihydrate was dissolved in 20 mL of 5% sodium hydroxide solution. Then, 5 mL of 30% hydrogen peroxide was slowly added under continuous stirring, and the mixture was stirred for another 0.5 h. The resulting precipitate was centrifuged and washed five times with deionized water. The precipitate was then dried in an oven at 60°C. Finally, the ZnO_2 product was ground into a fine powder using an agate mortar.

2.2 Preparation of CS@ZnO_2

1 g of chitosan was dissolved in 20 mL of 2% acetic acid solution. Then, 10 mg of zinc acetate dihydrate was slowly added under continuous stirring, and the mixture was stirred for another 0.5 h. The resulting mixture was then freeze-dried to obtain chitosan-zinc ion complexes. Next, 25 mL of 5% sodium hydroxide solution was added to the chitosan-zinc ion complexes, and then 5 mL of 30% hydrogen peroxide was slowly added and reacted for a period. The mixture was then washed with deionized water to neutral pH. The CS@ZnO_2 was obtained.

2.3 Characterization

Scanning electron microscopy (SEM) images were obtained from a Sigma 300 field emission scanning electron microscope (Carl Zeiss AG, Germany). Ultraviolet-visible (UV-vis) spectra were acquired on a UV-2450 spectrophotometer (Shimadzu Corporation, Japan). Fourier transform infrared (FT-IR) spectra were recorded via a Nicolet IS 5 Fourier transform infrared spectrometer (Thermo Fisher Scientific Inc., United States). X-ray diffraction (XRD) spectra were obtained from an Ultima IV X-ray diffractometer (Rigaku Holdings Corporation, Japan). X-ray photoelectron spectroscopy (XPS) was obtained by Thermo Scientific K-Alpha XPS (Thermo Fisher Scientific Inc., United States). Inductively coupled plasma mass spectrometry (ICP-MS) was obtained by Agilent 7,700x ICP-MS (Agilent Technologies Inc., United States). Confocal fluorescence imaging was performed using Leica TCS SP8 confocal luminescence microscope (Leica Microsystems Inc., Germany).

2.4 Characterization of peroxide groups

The peroxides groups of CS@ZnO_2 were verified by a $KMnO_4$ colorimetric assay. Briefly, CS@ZnO_2 was added to $KMnO_4$ solution (0.4 mM in 1 mM H_2SO_4). After incubation for 1 min, the color change of the solution was observed and the UV-vis absorption spectra were recorded immediately.

The production of ROS was confirmed using the 3,3′,5,5′-tetramethylbenzidine (TMB) colorimetric assay. Briefly, CS@ZnO_2 was added to 0.5 mM TMB solutions at different pH values (pH 3, 5, 7, and 9). After incubation for 30 min at 37°C, the color change of the solution was observed and the UV-vis absorption spectra were recorded immediately.

Furthermore, titanium oxysulfate ($TiOSO_4$) was selected as an indicator for H_2O_2 generation. $TiOSO_4$ reacts with H_2O_2 to form a primrose yellow titanium peroxide complex ($Ti(IV)O_2^{2+}$), which exhibits UV-vis absorbance at 405 nm. Specifically, CS@ZnO_2 was incubated in a pH five buffer solution for 2 h. Then, 0.5 mL of $TiOSO_4$ (0.03 M) solution was added to 0.5 mL of the supernatant, followed by further incubation for 10 min to produce the yellow $Ti(IV)O_2^{2+}$ precipitate. $Ti(IV)O_2^{2+}$ precipitate was collected by centrifugation at 13,000 rpm for 5 min and re-dissolved in 1 mL H_2SO_4 (1 M) solution, and the UV-vis absorption spectra were recorded immediately.

2.5 Characterization of the liquid absorption performance of CS@ZnO_2

The synthesized CS@ZnO_2 was dried, and their mass was measured. Digital photographs of the dried samples were also taken for documentation. Subsequently, the CS@ZnO_2 was subjected to compression under an external force, and the morphological changes were observed and recorded. Finally, the CS@ZnO_2 were reintroduced into pure water, and the weight change after water absorption was measured.

2.6 Bacterial culture

Escherichia coli ATCC25922 (*E. coli*) and *S. aureus* ATCC6538 (*S. aureus*) were selected as model Gram-negative and Gram-positive bacteria, respectively. Bacterial cells were grown overnight in LB medium (Luria-Bertani broth, Lennox modification) at 37°C and then harvested at the exponential growth phase via centrifugation. *E. coli* or *S. aureus* cells were washed twice to remove residual macromolecules and other growth medium constituents and re-suspended in sterile saline solution (0.9% NaCl). Bacterial suspensions with an optical density at 600 nm (OD600 nm) of 0.1 were used for the subsequent experiments.

2.7 Biocompatibility evaluation

Fresh human blood (ethical approval no. CSSDSYY-YXLL-SC-2023–03–20) was collected in heparinized tubes and centrifuged (3,000 rpm, 10 min) to isolate erythrocytes. Subsequently, the erythrocyte suspension (2% v/v) was incubated with CS@ZnO_2 solutions at 37°C for 4 h. Positive control (pure water) and negative control (0.9% NaCl solution) were included. After incubation, the samples were centrifuged again at 3,000 rpm for 10 min, and the absorbance of the supernatant was measured at a wavelength of 540 nm. The hemolysis ratio was calculated as follows:

$$\text{Hemolysis ratio (\%)} = \frac{OD_{sample} - OD_{negative}}{OD_{positive} - OD_{negative}} \times 100\%$$

2.8 Antibacterial assay

CS@ZnO_2 was added to the bacteria suspensions, and then the mixture was incubated at 37°C with shaking at 200 rpm for 24 h. The antibacterial property of CS@ZnO_2 was determined through the plate spreading experiment. Following the antibacterial experiments, the bacteria were harvested via centrifugation and subsequently washed with phosphate-buffered saline (PBS). According to the instructions of the bacterial viability assay kit (Beyotime Biotechnology, China), the samples were incubated with N,N-dimethylaniline N-oxide (DMAO) and propidium iodide (PI). In this process, viable bacteria were labeled with DMAO, producing green fluorescence, while non-viable bacteria were additionally stained with PI, resulting in red fluorescence emission. To distinguish between live and dead cells, confocal laser scanning microscopy was employed for imaging analysis.

To evaluate the production of reactive oxygen species (ROS) induced by CS@ZnO_2, the 2′,7′-dichlorodihydrofluorescein diacetate (DCFH-DA) assay was employed. In this process, the CS@ZnO_2 treated bacteria were incubated with DCFH-DA following the protocol provided in the ROS assay kit (Beyotime Biotechnology, China). Notably, DCFH-DA lacks fluorescence and can permeate bacterial cell membranes freely. Once inside the cells, it undergoes hydrolysis mediated by intracellular esterases, leading to the formation of DCFH, a compound that cannot exit the cells. Subsequently, intracellular ROS oxidize the non-fluorescent DCFH into fluorescent DCF. The intensity of DCF fluorescence serves as an indicator of the concentration of intracellular ROS.

3 Results and discussion

3.1 Antibacterial design strategies

The CS@ZnO_2 nanocomposite, designed in this study, demonstrates remarkable stability under neutral conditions due to its chitosan shell. Chitosan, a natural polysaccharide derived from chitin, is known for its biocompatibility and biodegradability. This protective layer ensures that the ZnO_2 remains intact and stable in physiological environments, preventing premature release or degradation. However, when exposed to slightly acidic conditions, such as those found in areas of bacterial infection, the chitosan shell exhibits acid-responsive dissociation (Hageman et al., 2024). This property is crucial because many pathogenic bacteria create a microenvironment with lower pH levels as they proliferate. Upon encountering these acidic conditions, the chitosan shell begins to break down, releasing the encapsulated ZnO_2 *in situ*. Once released, ZnO_2 undergoes self-decomposition under acidic conditions. This process leads to the generation of H_2O_2 (Elbahri et al., 2017). H_2O_2 is a potent antimicrobial agent that can generate ROS. These ROS cause irreversible damage to bacterial cellular components, including proteins and DNA, effectively eliminating the pathogens without inducing drug resistance (Zhu et al., 2021; Jannesari et al., 2023; Wang et al., 2023).

3.2 Characterization of CS@ZnO_2

The synthesis of ZnO_2 was characterized using XRD and the result is shown in Figure 1A. The diffraction peaks at 2θ = 31.9°, 37.0°, 53.2°, 63.3°, and 66.6° correspond to the (111) (200) (220) (311), and (222) of ZnO_2 (JCPDS card no. 13–0,311) respectively. The calculated d-values for these planes (2.80 Å, 2.43 Å, 1.72 Å, 1.47 Å and 1.40 Å) are in good agreement with the reference data. CS@ZnO_2 was further characterized using infrared absorption spectroscopy (FT-IR). As shown in Figure 1B, CS@ZnO_2 exhibits a characteristic peroxide (-O_2^{2-}) ion O-O bond absorption peak at 1,414 cm^{-1} (Huang et al., 2022). Additionally, there are obvious characteristic absorption peaks at 2,920 cm^{-1} and 2,970 cm^{-1}, which are attributed to the asymmetric and symmetric stretching vibration peaks of -CH_2- of chitosan, respectively (Ding et al., 2022; García Cambón et al., 2023). The morphology of CS@ZnO_2 was

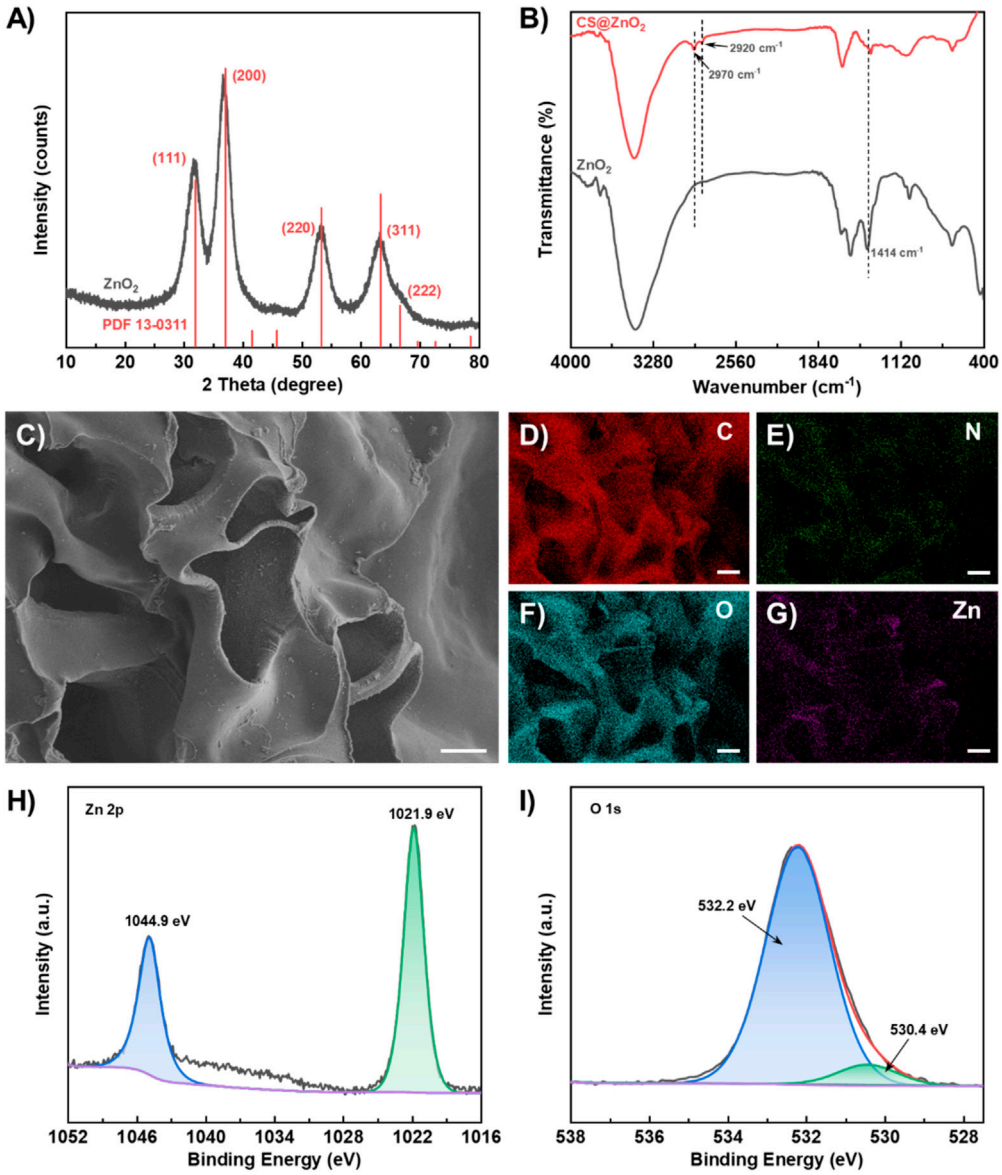

FIGURE 1
Characterization of CS@ZnO_2. **(A)** XRD pattern, **(B)** FT-IR spectra, **(C)** SEM image, **(D–G)** Elemental mapping images of C, O, N, and Zn, **(H)** Zn 2p spectrum and **(I)** O 1s spectrum.

characterized using scanning electron microscopy (SEM), and the results are shown in Figure 1C. The synthesized CS@ZnO_2 exhibit a porous structure, which enhances their capacity for liquid absorption. Additionally, granular substances have been observed to be embedded in the chitosan substrate. The elemental mapping analysis via SEM coupled with energy-dispersive X-ray spectroscopy (EDS) demonstrates a homogeneous spatial distribution of C, N, O, and Zn throughout the CS@ZnO_2 (Figures 1D–G). Quantitative analysis reveals that the atomic percentages of these elements are 60.04%, 10.32%, 29.13% and 0.51%, respectively (Supplementary Figure S1). The X-ray photoelectron spectroscopy (XPS) full-scan and high-resolution spectra were collected to investigate the chemical states of the CS@ZnO_2. As shown in Supplementary Figure S2, the XPS survey spectrum confirms the coexistence of C, N, O, and Zn, with their characteristic peaks appearing at binding energies of 285.7 eV, 398.9 eV, 532.2 eV and 1,021.9 eV, respectively. The Zn 2p spectrum (Figure 1H) exhibits spin-orbit splitting peaks at 1,021.9 eV ($2p_{3/2}$) and 1,044.9 eV ($2p_{1/2}$), which is consistent with the characteristic of Zn(II) oxide (Lin et al., 2019; Zhang et al., 2022). High-resolution scans of the O 1s region (Figure 1I) were deconvoluted into two distinct components using Gaussian-Lorentzian fitting. The dominant peak at 532.2 eV corresponds to O_2^{2-}, while the minor peaks at 530.4 eV is attributed to O^{2-}, indicating the presence of peroxide groups (Lin et al., 2019; Zhang et al., 2022). Quantitative analysis based on peak area ratios indicates that the O_2^{2-} accounts for

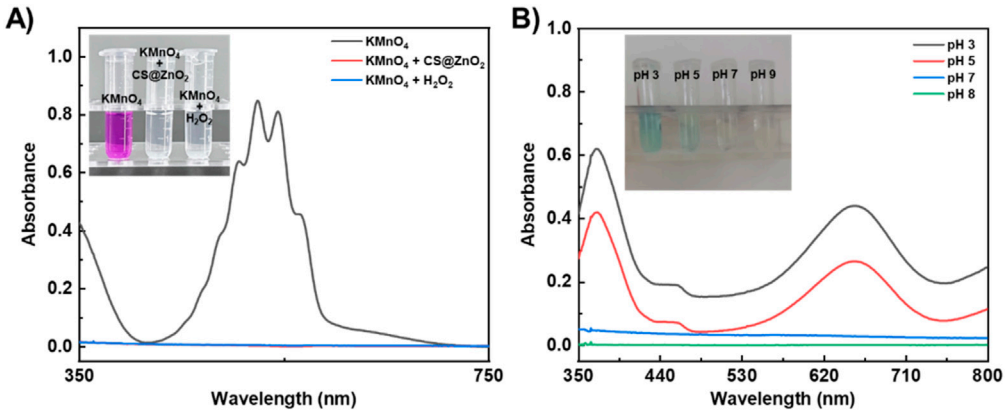

FIGURE 2
Acid-responsive self-decomposition properties of $CS@ZnO_2$. **(A)** Absorption spectra and photograph (inset) of $KMnO_4$ (in 1 M H_2SO_4) solution after incubation with $CS@ZnO_2$ or H_2O_2. **(B)** Absorption spectra and photograph (inset) of TMB solution after incubation with $CS@ZnO_2$ at different pH buffers.

92.2% of the total O 1s content. The above results indicate that the $CS@ZnO_2$ was successfully synthesized.

3.3 Acid-induced $CS@ZnO_2$ generates ROS

The classic redox reaction between potassium permanganate and hydrogen peroxide was used to determine whether ZnO_2 would self-decompose to release H_2O_2 under acidic conditions (Zhang et al., 2016; Sun et al., 2019). As expected (Figure 2A), the purple solution of acidic $KMnO_4$ became colourless and the characteristic absorption peaks disappeared after the addition of H_2O_2 or ZnO_2. This is because the H_2O_2 can reduce the purple MnO_4^- to colourless Mn^{2+} in acidic media (Equation 1), while ZnO_2 can self-decompose and release H_2O_2 under acidic conditions. These results further demonstrate the successful preparation of ZnO_2 and the nature of its self-decomposition to release H_2O_2 under acidic conditions. Furthermore, the concentration of released H_2O_2 was quantitatively determined using the titanium oxysulfate colorimetric method (Zhang et al., 2018; Gong et al., 2021). Based on the standard curve constructed with the standard H_2O_2 concentrations (Supplementary Figure S3), the amount of released H_2O_2 was calculated to be 287.7 ± 54.3 μM.

$$\mathbf{2MnO_4^- + 5H_2O_2 + 6H^+ \rightarrow 2Mn^{2+} + 5O_2 \uparrow + 8H_2O} \quad (1)$$

Taking advantage of the property that the colourless 3,3′,5,5′-tetramethylbenzidine (TMB) can be oxidized by ROS (such as OH^-) to form a blue TMB oxide (ox-TMB) with a strong absorption peak at 652 nm (Song et al., 2019; Aham et al., 2025; Wang et al., 2025), the ability of acid-induced $CS@ZnO_2$ to generate ROS was confirmed. As expected (Figure 2B), under weakly acidic conditions (pH 5), $CS@ZnO_2$ turned the TMB solution blue (inset of Figure 2B), and showed a strong absorption peak at 652 nm. This phenomenon was attributed to the self-decomposition of $CS@ZnO_2$ under weakly acidic conditions and the release of H_2O_2. Subsequently, H_2O_2 decomposed to produce ROS, such as OH^-, which oxidized TMB to form the blue ox-TMB. In addition, the intensity of the absorption peak at 652 nm and the blue color of the solution increased with the acidity (e.g., pH 3), indicating that the acidic environment was conducive to the decomposition of ZnO_2 in $CS@ZnO_2$ and promoted the production of more ROS. Conversely, the absorbance and color of the TMB solution remained basically unchanged at pH 7, suggesting that $CS@ZnO_2$ remained relatively stable under neutral conditions.

The above results indicate that the self-decomposition of ZnO_2 in $CS@ZnO_2$ can be activated under weak acidic conditions. By utilizing the acidic microenvironment (pH 5.0–6.0) associated with bacterial infection, the self-decomposition of ZnO_2 in $CS@ZnO_2$ can be triggered to release H_2O_2 and ROS on demand. $CS@ZnO_2$ demonstrates significant potential for the treatment of bacterial infections.

Notably, research indicates that the released Zn^{2+} also exhibit antibacterial properties due to their significant inhibition of the active transport process in microbial cells, interference with amino acid metabolic pathways, and disruption of enzyme systems (Sirelkhatim et al., 2015). The Zn^{2+} concentration released from $CS@ZnO_2$ under neutral (pH 7) and acidic (pH 5) conditions after 24 h of incubation was quantitatively characterized using inductively coupled plasma mass spectrometry (ICP-MS). The results demonstrated concentrations of released Zn^{2+} were 9.2 μM and 58.6 μM under neutral and acidic conditions, respectively. Previous studies have shown that bacteria have a certain tolerance to low concentrations of Zn^{2+}, and only when the Zn^{2+} concentration reaches the millimolar level will it exhibit significant toxic effects on bacteria (Xiong and Jayaswal, 1998; Outten and O'Halloran, 2001; Reddy et al., 2007). Combined with the ICP-MS results, it can be inferred that the released Zn^{2+} does not contribute to the antibacterial performance of $CS@ZnO_2$.

3.4 The liquid absorption performance of $CS@ZnO_2$

Another important step in the management of bacterially infected wounds is "drainage," which involves removing any fluid

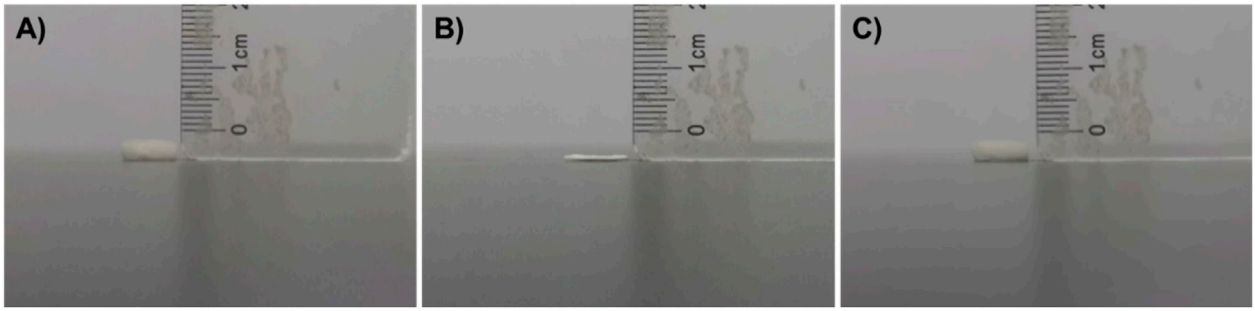

FIGURE 3
Characterization of CS@ZnO_2 hydrogels. Photographs of the CS@ZnO_2 in **(A)** the original state, **(B)** the force-compressed state, and **(C)** the shape-recovered state after water absorption.

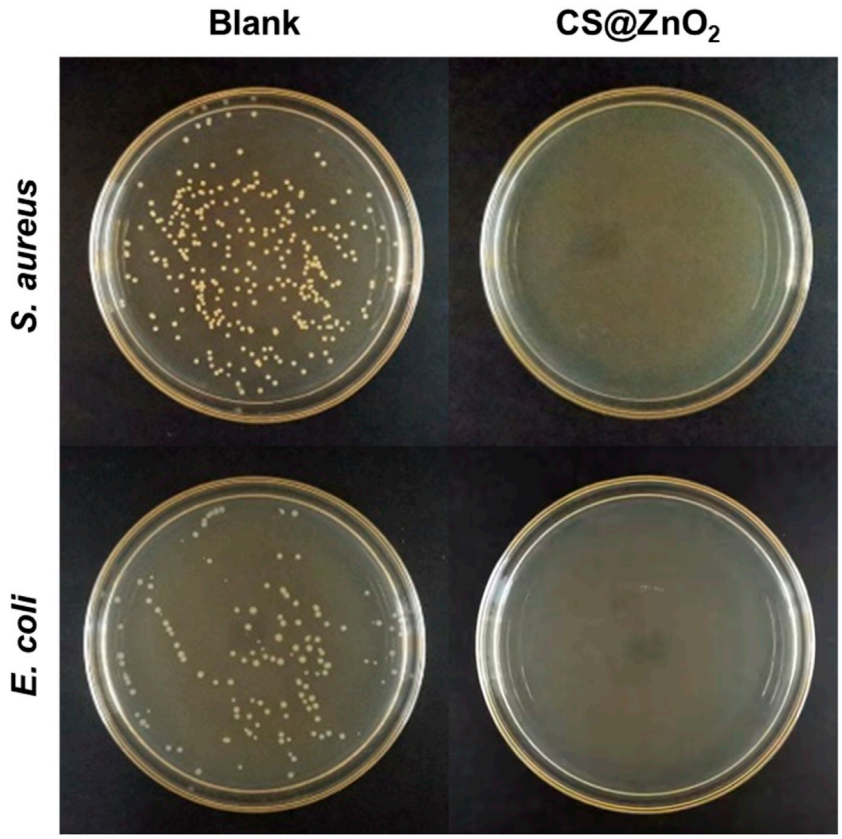

FIGURE 4
Antibacterial properties of CS@ZnO_2 against *Staphylococcus aureus* and *Escherichia coli*.

that has accumulated on the wound and directing it to an external dressing (Zerbe et al., 1996; Mellinghoff et al., 2019). This helps to remove bacteria from the wound and allows nutrients from the blood to be transported to the wound to promote healing (Williams and Barbul, 2012; Powers et al., 2016). Therefore, the absorption performance of the synthesized CS@ZnO_2 was evaluated through a water absorption test.

As shown in Figure 3, CS@ZnO_2 has a naturally fluffy appearance and a large volume. When subjected to external compression, the size and volume of CS@ZnO_2 were significantly reduced (Figures 3A, B). However, after reabsorption of water, CS@ZnO_2 can return to its original state (Figure 3C), indicating excellent liquid absorption and compression recovery properties. In addition, the water absorption capacity was assessed by measuring the mass of CS@ZnO_2 before and after water absorption. The results show that CS@ZnO_2 can absorb up to 27.2 times its dry weight (dry weight is 7.4 mg, wet weight is 208.8 mg), highlighting its superior liquid absorption performance and significant potential for medical applications.

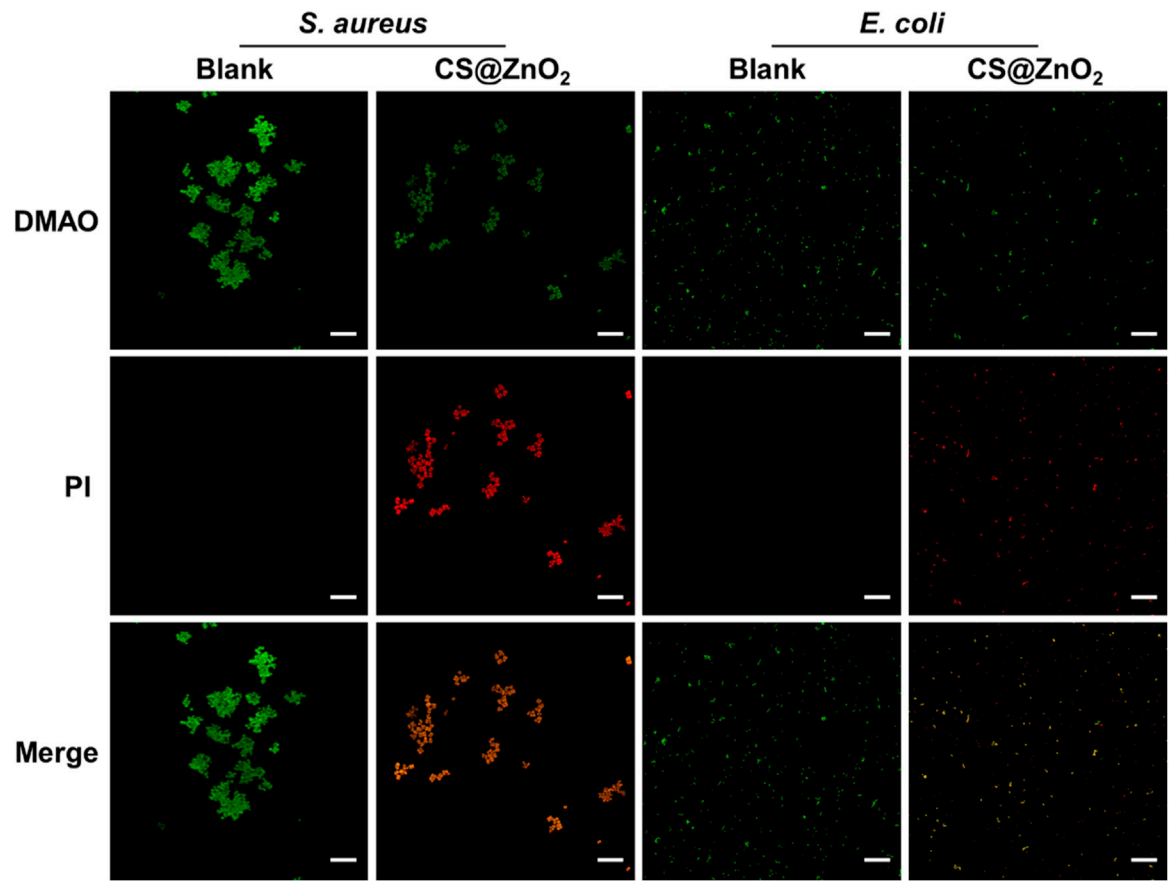

FIGURE 5
Confocal laser scanning microscopy images. CLSM images of *Staphylococcus aureus* and *Escherichia coli* after incubation with or without CS@ZnO_2. Stained with DMAO (green) and PI (red), scale bars = 25 μm.

3.5 The antibacterial properties of CS@ZnO_2

To biocompatibility of CS@ZnO_2 was investigated through hemolysis tests to verify its safety and potential value in biomedical applications. As shown in Supplementary Figure S4, the solution of the positive control group exhibited a distinct red coloration, whereas no visible color change was observed in either the negative control group or the CS@ZnO_2 experimental group. Quantitative assessment of hemolytic activity revealed a remarkably low hemolysis rate of 1.16% ± 0.25% for the CS@ZnO_2 group, demonstrating exceptional blood compatibility that complies with the stringent <5% safety criterion for biomedical devices outlined in ISO 10993–4.

Staphylococcus aureus, a typical Gram-positive bacterium, is known to cause many serious infections. *E. coli*, a typical Gram-negative bacterium, is also associated with numerous severe infections. In this experiment, the antimicrobial properties of CS@ZnO_2 against both Gram-positive and Gram-negative bacteria were investigated, using *S. aureus* and *E. coli* as representatives, respectively. Specifically, CS@ZnO_2 was co-incubated with the bacteria for 24 h, and the antibacterial effect was evaluated by the plate count method. As shown in Figure 4S *Aureus* exhibited significant colony formation in the control group, while no colonies were observed after incubation with CS@ZnO_2. Similarly, *E. coli* demonstrated robust colony formation in the control group, and no colonies were observed after incubation with CS@ZnO_2 either. These results indicate that CS@ZnO_2 exhibits excellent antibacterial performance.

To further evaluate the antimicrobial efficacy of CS@ZnO_2, bacterial viability was assessed through differential fluorescence staining. N,N-dimethylaniline N-oxide (DMAO), a green fluorescent nucleic acid dye, is capable of staining both live and dead bacteria due to its membrane-permeable properties. Propidium iodide (PI), in contrast, is a non-permeable fluorescent dye that cannot penetrate intact cell membranes of viable cells, making it ineffective for staining bacteria with undamaged membranes. However, in necrotic bacteria where membrane integrity is compromised, PI can enter the nucleus, bind to double-stranded DNA, intercalate into the DNA double helix, and form a PI-DNA complex, resulting in red fluorescence. When DMAO and PI are used in combination to detect the viability of bacteria, live bacteria with intact cell membranes exhibit only green fluorescence, whereas dead bacteria with damaged cell membranes display both green and red fluorescence. As shown in Figure 5, the blank group exhibited exclusively green fluorescence without any detectable red fluorescence, indicating that the bacteria were viable. In contrast, bacteria exposed to CS@ZnO_2 exhibited both green fluorescence and red fluorescence, suggesting that the bacteria membranes had been

compromised and the cells inactivated. These results demonstrate that CS@ZnO_2 possesses significant antibacterial properties.

The generation of reactive oxygen species in bacteria after treatment with CS@ZnO_2 was monitored using DCFH-DA. As shown in Supplementary Figure S5, compared with the untreated control group, bacteria exposed to CS@ZnO_2 exhibited significantly enhanced fluorescence intensity, indicating that CS@ZnO_2 can effectively stimulate the generation of ROS. The increase in ROS levels in the CS@ZnO_2 treatment group may be due to the *in-situ* decomposition of ZnO_2, which promotes the release of hydrogen peroxide and further enhances the generation of ROS. Such high concentrations of ROS damage bacterial membranes and intracellular components (such as DNA and proteins), ultimately leading to bacterial apoptosis.

4 Conclusion

In summary, CS@ZnO_2 with acid-responsive properties has been successfully synthesized and exhibit significant antibacterial performance. The synthesized CS@ZnO_2 remains stable under neutral conditions due to its chitosan shell, while it undergoes acid-responsive dissociation in the acidic microenvironment of bacterial infections. Following the dissociation of the chitosan shell, ZnO_2 is released *in situ* and subsequently decomposes under acidic conditions to produce bactericidal H_2O_2. The decomposition of H_2O_2 irreversibly damages bacteria, thereby achieving effective antibacterial activity without inducing bacterial resistance. This study provides a theoretical foundation for the development of novel clinical nano-antimicrobial agents and offers a basis for their further application in combating bacterial infections.

Data availability statement

The original contributions presented in the study are included in the article/Supplementary Material, further inquiries can be directed to the corresponding author.

Ethics statement

The studies involving humans were approved by The Medical Ethics Committee of the Fourth Hospital of Changsha. The studies were conducted in accordance with the local legislation and institutional requirements. The participants provided their written informed consent to participate in this study.

Author contributions

YZ: Conceptualization, Data curation, Formal Analysis, Funding acquisition, Investigation, Methodology, Writing – original draft, Writing – review and editing. JL: Data curation, Formal Analysis, Writing – original draft. SL: Data curation, Formal Analysis, Writing – original draft. JZ: Formal Analysis, Validation, Writing – review and editing. JL: Formal Analysis, Validation, Writing – review and editing. YH: Project administration, Resources, Supervision, Writing – review and editing.

Funding

The author(s) declare that financial support was received for the research and/or publication of this article. This work was supported by the Research Project of Changsha Municipal Health Commission (KJ-B2023068).

Conflict of interest

The authors declare that the research was conducted in the absence of any commercial or financial relationships that could be construed as a potential conflict of interest.

Generative AI statement

The author(s) declare that no Generative AI was used in the creation of this manuscript.

Publisher's note

Supplementary material

The Supplementary Material for this article can be found online at: https://www.frontiersin.org/articles/10.3389/fbioe.2025.1608188/full#supplementary-material

References

Aham, E. C., Ravikumar, A., Arunjegan, A., Tamilselvan, G., Hu, Z., Xiao, J., et al. (2025). Smartphone-integrated colorimetric sensor for rapid detection of phenolic compounds based on the peroxidase-mimicking activity of copper/cerium-aspartic acid metal–organic framework. *Microchim. Acta* 192 (1), 51. doi:10.1007/s00604-024-06873-5

Bai, S., Lan, Y., Fu, S., Cheng, H., Lu, Z., and Liu, G. (2022). Connecting calcium-based nanomaterials and cancer: from diagnosis to therapy. *Nano-Micro Lett.* 14 (1), 145. doi:10.1007/s40820-022-00894-6

Bi, X., Bai, Q., Liang, M., Yang, D., Li, S., Wang, L., et al. (2022). Silver peroxide nanoparticles for combined antibacterial sonodynamic and photothermal therapy. *Small* 18 (2), 2104160. doi:10.1002/smll.202104160

Cao, M., Wang, S., Hu, J.-H., Lu, B.-H., Wang, Q.-Y., and Zang, S.-Q. (2022). Silver cluster-porphyrin-assembled materials as advanced bioprotective materials for combating superbacteria. *Adv. Sci.* 9 (2), 2103721. doi:10.1002/advs.202103721

Chen, H., Li, Y., Chen, D., Fang, Y., Gong, X., Wang, K., et al. (2024). Photothermally enhanced antibacterial wound healing using albumin-loaded tanshinone IIA and

IR780 nanoparticles. *Front. Bioeng. Biotechnol.* 12, 1487660. doi:10.3389/fbioe.2024.1487660

Cook, M. A., and Wright, G. D. (2022). The past, present, and future of antibiotics. *Sci. Transl. Med.* 14 (657), eabo7793. doi:10.1126/scitranslmed.abo7793

Davies, J., and Davies, D. (2010). Origins and evolution of antibiotic resistance. *Microbiol. Mol. Biol. Rev.* 74 (3), 417–433. doi:10.1128/mmbr.00016-10

Ding, X., Zhao, L., Khan, I. M., Yue, L., Zhang, Y., and Wang, Z. (2022). Emerging chitosan grafted essential oil components: a review on synthesis, characterization, and potential application. *Carbohydr. Polym.* 297, 120011. doi:10.1016/j.carbpol.2022.120011

Dong, Y., and Wang, Z. (2023). ROS-scavenging materials for skin wound healing: advancements and applications. *Front. Bioeng. Biotechnol.* 11, 1304835. doi:10.3389/fbioe.2023.1304835

Elbahri, M., Abdelaziz, R., Disci-Zayed, D., Homaeigohar, S., Sosna, J., Adam, D., et al. (2017). Underwater Leidenfrost nanochemistry for creation of size-tailored zinc peroxide cancer nanotherapeutics. *Nat. Commun.* 8 (1), 15319. doi:10.1038/ncomms15319

García Cambón, T. A., Lopez, C. S., Hanheiser, N., Bhatia, S., Achazi, K., Rivas, M. V., et al. (2023). Benzoxaborole-grafted high molecular weight chitosan from prawn: synthesis, characterization, target recognition and antibacterial properties. *Carbohydr. Polym.* 316, 120925. doi:10.1016/j.carbpol.2023.120925

Gong, M., Xiao, J., Li, H., Hai, L., Yang, K., Li, J., et al. (2021). Magnetically retained and glucose-fueled hydroxyl radical nanogenerators for H_2O_2-self-supplying chemodynamic therapy of wound infections. *Mater. Sci. Eng. C* 131, 112522. doi:10.1016/j.msec.2021.112522

Hageman, K. A., Blatt, R. L., Kuenne, W. A., Brow, R. K., and McIff, T. E. (2024). Effect of pH and hydroxyapatite-like layer formation on the antibacterial properties of borophosphate bioactive glass incorporated poly(methyl methacrylate) bone cement. *Front. Bioeng. Biotechnol.* 12, 1462795. doi:10.3389/fbioe.2024.1462795

Huang, K., Li, F., Yuan, K., Yang, Y., Chang, H., Liang, Y., et al. (2022). A MOF-armored zinc-peroxide nanotheranostic platform for eradicating drug resistant bacteria *via* image-guided and *in situ* activated photodynamic therapy. *Appl. Mater. Today* 28, 101513. doi:10.1016/j.apmt.2022.101513

Hwang, C., Choi, M.-H., Kim, H.-E., Jeong, S.-H., and Park, J.-U. (2022). Reactive oxygen species-generating hydrogel platform for enhanced antibacterial therapy. *NPG Asia Mater.* 14 (1), 72. doi:10.1038/s41427-022-00420-5

Jannesari, M., Akhavan, O., Madaah Hosseini, H. R., and Bakhshi, B. (2023). Oxygen-rich graphene/ZnO_2-Ag nanoframeworks with pH-switchable catalase/peroxidase activity as O_2 nanobubble-self generator for bacterial inactivation. *J. Colloid Interface Sci.* 637, 237–250. doi:10.1016/j.jcis.2023.01.079

Lin, L.-S., Wang, J.-F., Song, J., Liu, Y., Zhu, G., Dai, Y., et al. (2019). Cooperation of endogenous and exogenous reactive oxygen species induced by zinc peroxide nanoparticles to enhance oxidative stress-based cancer therapy. *Theranostics* 9 (24), 7200–7209. doi:10.7150/thno.39831

Liu, B., Bian, Y., Liang, S., Yuan, M., Dong, S., He, F., et al. (2022). One-step integration of tumor microenvironment-responsive calcium and copper peroxides nanocomposite for enhanced chemodynamic/ion-interference therapy. *ACS Nano* 16 (1), 617–630. doi:10.1021/acsnano.1c07893

Makabenta, J. M. V., Nabawy, A., Li, C.-H., Schmidt-Malan, S., Patel, R., and Rotello, V. M. (2021). Nanomaterial-based therapeutics for antibiotic-resistant bacterial infections. *Nat. Rev. Microbiol.* 19 (1), 23–36. doi:10.1038/s41579-020-0420-1

Mellinghoff, S. C., Otto, C., and Cornely, O. A. (2019). Surgical site infections: current management and role of new antibiotics. *Curr. Opin. Infect. Dis.* 32 (5), 517–522. doi:10.1097/qco.0000000000000589

Outten, C. E., and O'Halloran, T. V. (2001). Femtomolar sensitivity of metalloregulatory proteins controlling zinc homeostasis. *Science* 292 (5526), 2488–2492. doi:10.1126/science.1060331

Powers, J. G., Higham, C., Broussard, K., and Phillips, T. J. (2016). Wound healing and treating wounds: chronic wound care and management. *J. Am. Acad. Dermatology* 74 (4), 607–625. doi:10.1016/j.jaad.2015.08.070

Reddy, K. M., Feris, K., Bell, J., Wingett, D. G., Hanley, C., and Punnoose, A. (2007). Selective toxicity of zinc oxide nanoparticles to prokaryotic and eukaryotic systems. *Appl. Phys. Lett.* 90 (21), 2139021–2139023. doi:10.1063/1.2742324

Sirelkhatim, A., Mahmud, S., Seeni, A., Kaus, N. H. M., Ann, L. C., Bakhori, S. K. M., et al. (2015). Review on zinc oxide nanoparticles: antibacterial activity and toxicity mechanism. *Nano-Micro Lett.* 7 (3), 219–242. doi:10.1007/s40820-015-0040-x

Song, H., Li, X., He, Y., Peng, Y., Pan, J., Niu, X., et al. (2019). Colorimetric evaluation of the hydroxyl radical scavenging ability of antioxidants using carbon-confined CoOx as a highly active peroxidase mimic. *Microchim. Acta* 186 (6), 354. doi:10.1007/s00604-019-3488-4

Stojanov, S., Kristl, J., Zupančič, Š., and Berlec, A. (2022). Influence of excipient composition on survival of vaginal lactobacilli in electrospun nanofibers. *Pharmaceutics* 14 (6), 1155. doi:10.3390/pharmaceutics14061155

Sun, L., Zhao, Y., Peng, H., Zhou, J., Zhang, Q., Yan, J., et al. (2024). Carbon dots as a novel photosensitizer for photodynamic therapy of cancer and bacterial infectious diseases: recent advances. *J. Nanobiotechnology* 22 (1), 210. doi:10.1186/s12951-024-02479-4

Sun, Y., Liu, H., Tan, X., Li, Z., Du, Y., Zheng, A., et al. (2019). Highly efficient redox reaction between potassium permanganate and 3,3′,5,5′-tetramethylbenzidine for application in hydrogen peroxide based colorimetric assays. *RSC Adv.* 9 (4), 1889–1894. doi:10.1039/C8RA07758D

Theuretzbacher, U., Baraldi, E., Ciabuschi, F., and Callegari, S. (2023). Challenges and shortcomings of antibacterial discovery projects. *Clin. Microbiol. Infect. official Publ. Eur. Soc. Clin. Microbiol. Infect. Dis.* 29 (5), 610–615. doi:10.1016/j.cmi.2022.11.027

Wang, D., Zhang, Y., Li, X., Lei, P., Shuang, S., and Dong, C. (2025). The smartphone-assisted sensing platform based on manganese dioxide nanozymes for the specific detection and degradation of hydroquinone. *J. Hazard. Mater.* 487, 137133. doi:10.1016/j.jhazmat.2025.137133

Wang, J., Qu, C., Shao, X., Song, G., Sun, J., Shi, D., et al. (2023). Carrier-free nanoprodrug for p53-mutated tumor therapy *via* concurrent delivery of zinc-manganese dual ions and ROS. *Bioact. Mater.* 20, 404–417. doi:10.1016/j.bioactmat.2022.06.005

Williams, J. Z., and Barbul, A. (2012). Nutrition and wound healing. *Crit. Care Nurs. Clin.* 24 (2), 179–200. doi:10.1016/j.ccell.2012.03.001

Xie, S., Li, G., Hou, Y., Yang, M., Li, F., Li, J., et al. (2020). A synergistic bactericidal effect of low-frequency and low-intensity ultrasound combined with levofloxacin-loaded PLGA nanoparticles on *M. smegmatis* in macrophages. *J. Nanobiotechnology* 18 (1), 107. doi:10.1186/s12951-020-00658-7

Xin, Q., Shah, H., Nawaz, A., Xie, W., Akram, M. Z., Batool, A., et al. (2019). Antibacterial carbon-based nanomaterials. *Adv. Mater.* 31 (45), 1804838. doi:10.1002/adma.201804838

Xiong, A., and Jayaswal, R. K. (1998). Molecular characterization of a chromosomal determinant conferring resistance to zinc and cobalt Ions in *Staphylococcus aureus*. *J. Bacteriol.* 180 (16), 4024–4029. doi:10.1128/jb.180.16.4024-4029.1998

Yang, N., Sun, M., Wang, H., Hu, D., Zhang, A., Khan, S., et al. (2024). Progress of stimulus responsive nanosystems for targeting treatment of bacterial infectious diseases. *Adv. Colloid Interface Sci.* 324, 103078. doi:10.1016/j.cis.2024.103078

Zerbe, M., McArdle, A., and Goldrick, B. (1996). Exposure risks related to the management of three wound drainage systems. *Am. J. Infect. Control* 24 (5), 346–352. doi:10.1016/s0196-6553(96)90021-8

Zhang, R., Feng, L., Dong, Z., Wang, L., Liang, C., Chen, J., et al. (2018). Glucose and oxygen exhausting liposomes for combined cancer starvation and hypoxia-activated therapy. *Biomaterials* 162, 123–131. doi:10.1016/j.biomaterials.2018.02.004

Zhang, Y., Gao, D., Fan, J., Nie, J., Le, S., Zhu, W., et al. (2016). Naked-eye quantitative aptamer-based assay on paper device. *Biosens. Bioelectron.* 78, 538–546. doi:10.1016/j.bios.2015.12.003

Zhang, Y., Liu, W., Huang, Y., Wang, Y., Chen, X., and Chen, Z. (2022). Bacterial biofilm microenvironment responsive copper-doped zinc peroxide nanocomposites for enhancing chemodynamic therapy. *Chem. Eng. J.* 446, 137214. doi:10.1016/j.cej.2022.137214

Zhu, Y., Wang, W., Cheng, J., Qu, Y., Dai, Y., Liu, M., et al. (2021). Stimuli-responsive manganese single-atom nanozyme for tumor therapy *via* integrated cascade reactions. *Angew. Chem. Int. Ed.* 60 (17), 9480–9488. doi:10.1002/anie.202017152